Inorganic Chemistry

ARTICLE

pubs.acs.org/IC

PH-Controlled Construction of Cu(I) Coordination Polymers: In Situ Transformation of Ligand, Network Topologies, and Luminescence and UV−vis-NIR Absorption Properties

Zhen-Lan Fang, Jian-Gang He, Qi-Sheng Zhang, Qi-Kai Zhang, Xiao-Yuan Wu, Rong-Min Yu, and Can-Zhong Lu*

The State Key Laboratory of Structural Chemistry, Fujian Institute of Research on the Structure of Matter, the Chinese Academy of Sciences, Fuzhou, Fujian, 350002, P.R. China

Supporting Information

ABSTRACT: Two new complexes $[Cu^{I}_{3}(L1)I_3]_n$ (**1**, L1 = 2,5-bis(4-pyridyl)-1,3,4-oxadiazole) and $[Cu^{I}_{3}(L2)I_2]_n$ (**2**, L2 = 2,5-bis(4-pyridyl)-1,2,4-triazolate) are controllably formed by using aqueous ammonia to regulate the pH value of the reaction involving CuI and L1. Interestingly, L2 of **2** is in situ generated from the ring transform of L1 when increase the pH value of the reaction. **1** exhibits 2-D layer, while **2** shows 3-D MOFs with a novel 3-nodal 4,4,5-connected net topology of an unprecedented Point (Schlafli) symbol: $(4\cdot5^2\cdot6^2\cdot7)(5^4\cdot8^2)(4^3\cdot5\cdot6^6)$. Although both **1** and **2** are built of CuI and similar ligands, different arrangements of CuI chains and ligands endow them with different physical properties. **1** displays a strong pure red luminescence emission, while **2** is nonluminescent and shows a broad absorption band covering the whole UV−vis-NIR spectrum range. The emissive excited states of **1** and the charge transitions of the optical absorption for **2** are solved by DFT calculations.

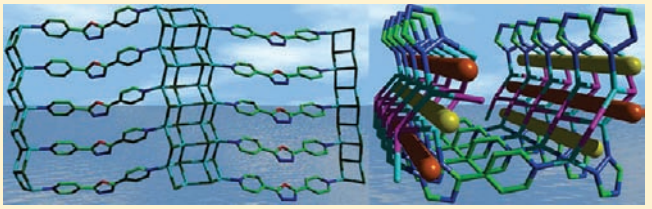

INTRODUCTION

The chemistry of coordination polymers[1] has attracted extensive interest owing to their intriguing architectures and topologies and great promise in a number of applications, including gas storage catalysis, magnetism, semiconductor, luminescence and nonlinear optics.[2] Over the past decades, a large variety of coordination polymers based on the linkage of metal ions (or clusters) with multidentate organic ligands have been reported. However, it is still difficult to design coordination polymers with interesting luminescence properties. The insertion of heavy metal centers (such as Ru^{2+}, Os^{2+}, Rh^{3+}, Ir^{3+}, Ag^{1+}) in coordination polymers can promote intersystem crossing to generate triplet states owing to the efficient spin−orbit coupling (consequence of the heavy atom effect), and therefore efficiently elongate the lifetime of excited state and increase the efficiency of solid-state emissions, making such heavy metal complexes of interest as potential luminescence materials. There are challenges in identifying the nature of the emitting states luminescence materials[3] because emission originates from a triplet has a large number of optical transitions possibility including metal-to-ligand-charge (MLCT) transfer, ligand-to-metal-charge-transfer (LMCT), and d−d electronic transitions (MMCT), etc.,[4] which do not occur in pure organic compounds. However, the density functional theory (DFT) calculations have been proved to be effective means of analysis charge transfer mechanism.[5] Besides Ru^{2+}, Ir^{3+}, or other noble metal complexes, luminescent/phosphorescent polymeric and polynuclear d^{10} metal (*i. e.* Cu^{+}, Ag^{+}) complexes, have attracted increasing interest due to their various advantages, such as resource-rich, low cost, and nontoxic properties, in applications ranging from organic light emitting devices (OLEDs) to biological sensors.[6] Among luminescence Cu^{I} complexes, those based on CuI are well-known for their structural diversity, rich photophysical behavior, and high luminescence efficiency.[7]

In situ hydro(solvo)thermal ligand synthesis reactions, as a new approach in crystal engineering, have been employed to synthesize metal−organic frameworks in the past decade.[8] The combination of hydrothermal methods with in situ synthesis has demonstrated increasing success in providing alternative pathways to crystalline complexes that are difficult to obtain by normal direct synthetic methods.[8f] Under hydro(solvo)thermal conditions, pH value, autogenous pressure, and relatively high temperature enhance the reactivity of the organic reagents and bring on complicated and unexpected but exciting results.[1d,8a,9] However, the precise mechanisms of most them have not been fully understood[8e] because of several phases involved in the products. Therefore, a lot of effort has been directed to obtain a single product by controlling the reaction conditions, such as time, temperature, solvent, pH value, stoichiometry and duration.[10] 1,3,4-Oxadiazole (Ox) and its derivatives exhibit considerably high electron affinities, which make them good candidates for electron injection and transportation in OLED devices. Recently, a series of metal coordination polymers based on oxadiazole derivatives have also been reported, however, to our knowledge,

Received: May 31, 2011
Published: October 21, 2011

Scheme 1. In Situ Metal/Ligand Solvothermal Reaction of CuI and L1

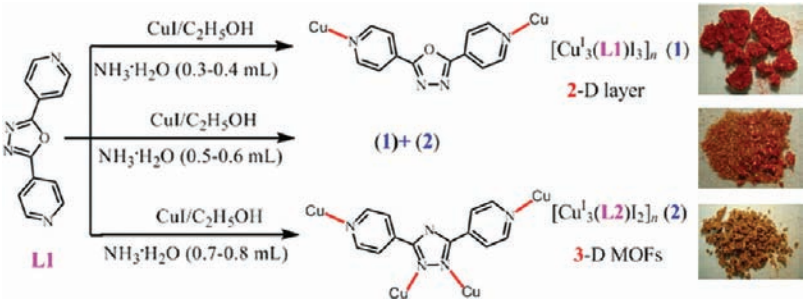

there is few pure red luminescence materials designed with oxadiazole derivatives. Therefore, we have applied the above-mentioned synthesis strategy and choose 1,3,4-oxadiazoles as the building blocks for the preparation of desirable complexes. The reaction of CuI and 2,5-bis(4-pyridyl)-1,3,4-oxadiazole (L1) with aqueous ammonia (0.5−0.6 mL; pH = 11.4−11.6) under solvothermal conditions generated mixed products $[Cu^{I}_{3}(L1)I_3]_n$ (**1**) and $[Cu^{I}_{3}(L2)I_2]_n$ (**2**, L2 = 2,5-bis(4-pyridyl)-1,2,4-triazolate). Interestingly, partial L1 in situ transformed to L2 during the process of this reaction. Most importantly, these two new complexes can be easily isolated when fine-tuning pH value through adjusting the volume of added aqueous ammonia.

EXPERIMENTAL SECTION

Materials and General Methods. The original bridging ligand (Scheme 1) was synthesized according to reported literature procedure.[11] Other chemicals were obtained from commercial sources, and used without further purification. The IR spectra (KBr pellets) were recorded on a Magna 750 FT-IR spectrophotometer in the range 400−4000 cm^{-1}. C, H, and N elemental analyses were determined on an EA1110 CHNS-0 CE element analyzer. Powder X-ray diffraction data were recorded on a PANaytical X'pert pro X-ray diffractometer with graphite-monochromatized Cu Kα radiation (λ = 1.542 Å). Optical diffuse reflectance spectra were measured at room temperature with a PE Lambda 35 UV−vis spectrophotometer. The instrument was equipped with an integrating sphere and controlled by a personal computer. The samples were ground into fine powder and then pressed onto a thin glass slide holder. A $BaSO_4$ plate was used as a standard (100% reflectance). The absorption spectra were calculated from reflectance spectra using the Kubelka−Munk function: $R/S = (1 - R)^2/(2R)$,[12] where R is the absorption coefficient, S is the scattering coefficient which is practically wavelength independent when the particle size is larger than 5 μm, and R is the reflectance. Thermal stability studies were carried out on a NETSCHZ STA 449C thermoanalyzer under N_2 (30−1200 °C range) at a heating rate of 10 K/min. Fluorescence spectra were measured on an Edinburgh Analytical instrument FLS920. The solid-state ^{13}C MAS NMR spectra were recorded on the Bruker DVANCE III 400 NMR spectrometer where the ^{13}C Larmor frequency is 100 MHz. The samples were spun at 3.0 kHz using a 4.0 mm Bruker double resonance MAS probe. The pH values of solutions were detected on a Starter 3C pH meter combined with a glass electrode. The pH meter was 3-point (pH = 6.86, 4.00, 9.18) calibrated through standard pH buffer solutions, and the measured pH values are accurate to ±0.01 pH units. In order to accurately measure the pH values of solutions, aqueous ammonia (25%) must be quickly added into the mixtures containing CuI (117.0 mg, 0.6 mmol), L1 (45.0 mg, 0.2 mmol), anhydrous ethanol (10 mL), and then sealed in a Parr Teflon-lined stainless steel vessel (20 mL). They were stirred at room temperature until uniformly dispersed, then the lids of reaction vessels were quickly opened and the mouths of reaction vessels were immediately sealed with plastic wrap. Finally, the pH meter electrode was inserted into the solutions, which were stirred in order to keep uniformly dispersed.

Table 1. Crystal Data and Structure Refinement Results for 1−2

complexes	**1**	**2**
empirical formula	$C_{12}H_8Cu_3I_3N_4O$	$C_{12}H_8Cu_3I_2N_5$
formula weight	795.54	666.65
cryst syst	monoclinic	monoclinic
space group	$P2_1/n$	$P2_1/c$
Z	4	4
a (Å)	17.581(2)	19.465(7)
b (Å)	4.1743(2)	4.083(2)
c (Å)	23.823(2)	19.122(7)
β (deg)	96.073(5)	91.555(7)
V (Å^3)	1738.5(2)	1519.2(1)
ρ_{calcd} (g/cm^3)	3.039	2.915
μ (mm^{-1})	8.969	8.226
GOF	1.087	1.058
R1 ($I > 2\sigma(I)$)[a]	0.043	0.049
wR2 (all data)[b]	0.082	0.190

[a] $R1 = \Sigma||F_o| - |F_c||/\Sigma|F_o|$. [b] $wR2 = \{\Sigma[w(F_o^2 - F_c^2)^2/\Sigma[w(F_o^2)^2]]\}^{1/2}$.

*Synthesis of $[Cu^{I}_{3}(L1)I_3]_n$ (**1**).* Aqueous ammonia (25%, 0.3−0.4 mL) was quickly added into the mixture containing CuI (117.0 mg, 0.6 mmol), L1 (45.0 mg, 0.2 mmol), anhydrous ethanol (10 mL), and then sealed in a Parr Teflon-lined stainless steel vessel (20 mL). It was stirred for 2 h at room temperature to make the mixed solution uniformly dispersed. And then it was heated at 180 °C for 72 h, followed by slow cooling to room temperature. Vermeil needle crystals of the product were collected, washed with H_2O, and air-dried in high yield (75.0% based on L1). Anal. Calcd (%) for $C_{12}H_8Cu_3I_3N_4O$: C, 18.10; H, 1.01; N, 7.04. Found: C, 18.36; H, 0.85; N, 7.08. FT-IR (solid KBr pellet, ν/cm^{-1}): 1614(s), 1563(m), 1532(m), 1481(s), 1422(s), 1383(m), 1328(m), 1277(m), 1230(w), 1211(m), 1121(w), 1058(m), 1012(m), 968(m), 835 (s), 742(s), 726(s), 710(s), 534(w), 507(m), 415(w).

*Synthesis of $[Cu^{I}_{3}(L2)I_2]_n$ (**2**).* A similar solvothermal reaction with aqueous ammonia increasing to 0.7−0.8 mL leds to L1 converted into L2, and resulted in the formation of brown crystals of **2** in 68.0% yield based on L1. Anal. Calcd (%) for $C_{12}H_8Cu_3I_2N_5$: C, 21.62; H, 1.21; N, 10.50. Found: C, 21.91; H, 1.23; N, 10.54. FT-IR (solid KBr pellet, ν/cm^{-1}): 1607(s), 1450(w), 1434(s), 1423(s), 1387(w), 1340(w), 1286(w), 1207(s), 1184(w), 1145(w), 1102(w), 1063(w), 1039(w), 1008(s), 996(w), 957(w), 863(w), 832(s), 750(s), 734 (s), 722(s), 711(w), 699(m), 668(w), 566(m),

dx.doi.org/10.1021/ic2011666 |*Inorg. Chem.* 2011, 50, 11403–11411

Table 2. Selected Bond Lengths (Å) and Angles (deg) for 1−2[a]

1			
Cu(1)−I(1)	2.701(1)	Cu(1)−I(2)	2.640(1)
Cu(1)−I(1)#6	2.690(1)	Cu(1)−I(1)#3	2.694(1)
Cu(2)−I(1)	2.715(1)	Cu(2)−I(2)#2	2.696(1)
Cu(2)−I(2)	2.601(1)	Cu(2)−N(4)	2.045(5)
Cu(3)−I(3)	2.614(1)	Cu(3)−I(3)#2	2.664(1)
Cu(3)−I(3)#4	2.647(1)	Cu(3)−N(1)	2.045(5)
Cu(1)−Cu(2)	2.916(1)	Cu(3)−Cu(3)#4	2.741(2)
Cu(1)#2−Cu(2)	2.912(1)	Cu(3)−Cu(3)#5	2.986(2)
Cu(1)−Cu(2)#3	2.912(1)	I(1)−Cu(1)−I(2)	113.22(4)
I(1)#6−Cu(1)−I(2)	107.45(4)	I(1)#6−Cu(1)−I(1)	109.41(4)
I(1)#3−Cu(1)−I(2)	115.60(4)	I(1)#6−Cu(1)−I(1)#3	109.60(4)
I(1)#3−Cu(1)−I(1)	101.39(4)	N(4)−Cu(2)−I(1)	105.88(16)
N(4)−Cu(2)−I(2)	118.14(16)	I(2)−Cu(2)−I(1)	114.01(4)
N(4)−Cu(2)−I(2)#2	101.22(16)	I(2)#2−Cu(2)−I(1)	113.06(4)
I(2)−Cu(2)−I(2)#2	103.98(4)	I(3)#4−Cu(3)−I(3)#2	111.58(4)
N(1)−Cu(3)−I(3)	109.55(18)	N(1)−Cu(3)−I(3)#2	105.00(17)
N(1)−Cu(3)−I(3)#4	108.27(16)	I(3)−Cu(3)−I(3)#2	104.55(4)
I(3)−Cu(3)−I(3)#4	117.20(4)		
2			
Cu(1)−I(2)	2.627(2)	Cu(1)−N(1)#7	1.966(7)
Cu(1)−I(2)#8	2.505(2)	Cu(2)−I(2)	2.714(2)
Cu(2)−N(5)	1.974(7)	Cu(2)−I(2)#4	3.088(2)
Cu(2)−N(2)#6	1.929(7)	Cu(3)−I(1)#2	2.689(2)
Cu(3)−N(4)	2.071(7)	Cu(3)−I(1)	2.627(2)
Cu(3)−I(1)#4	2.634(2)	Cu(1)−Cu(1)#3	2.994(2)
Cu(3)−Cu(3)#5	2.687(2)	Cu(3)−Cu(3)#2	2.927(3)
N(1)#7−Cu(1)−I(2)#8	126.4(2)	I(2)#8−Cu(1)−I(2)	125.23(7)
N(1)#7−Cu(1)−I(2)	106.5(2)	N(4)−Cu(3)−I(1)#4	111.1(2)
N(2)#6−Cu(2)−N(5)	139.4(3)	I(1)−Cu(3)−I(1)#4	101.81(6)
N(2)#6−Cu(2)−I(2)	110.2(2)	N(4)−Cu(3)−I(1)	108.8(2)
N(5)−Cu(2)−I(2)	108.6(2)	N(4)−Cu(3)−I(1)#2	102.5(2)
N(2)#6−Cu(2)−I(2)#4	97.9(2)	I(1)−Cu(3)−I(1)#2	113.19(5)
N(5)−Cu(2)−I(2)#4	94.1(2)	I(1)#4−Cu(3)−I(1)#2	119.38(4)
I(2)−Cu(2)−I(2)#4	89.20(5)		

[a] Symmetry transformations used to generate equivalent atoms. **1**: (#2) $x, y-1, z$; (#3) $x, y+1, z$; (#4) $-x+1, -y+2, -z+1$; (#5) $-x+1, -y+1, -z+1$; (#6) $-x+1/2, y+1/2, -z-1/2$. **2**: (#2) $-x, -y+1, -z+1$; (#3) $x, y+1, z$; (#4) $x, y+1, z$; (#5) $-x, -y+2, -z+1$; (#6) $x, -y+1/2, z-1/2$; (#7) $x, -y-1/2, z-1/2$; (#8) $-x+1, y-1/2, -z-1/2$.

538(w), 504(m), 449(m). Solid-state ^{13}C NMR (δ): 124.6, 138.9, 149.5, 163.7.

X-ray Crystallography. The single crystals of these complexes in present work were mounted on a glass fiber for the X-ray diffraction analysis. Diffraction data were collected at 293(2) K on a Rigaku AFC7R diffractometer using graphite-monochromated Mo-K_α radiation (λ = 0.71073 Å) from a rotating anode generator, and intensities were corrected for LP factors and empirical absorption using the ψ scan technique. The structures were solved by direct methods, developed by subsequent difference Fourier syntheses, and refined using the Siemens SHELXTL, version 5, software package.[13] All nonhydrogen atoms were refined with anisotropic displacement parameters. All H atoms on carbons were placed in calculated positions and refined using the riding model. Crystal data as well as details of data collection and refinement for **1**−**2** are summarized in Table 1. The selected interatomic distances and bond angles are given in Table 2.

Computational Descriptions. The crystallographic data of **1**−**2** determined by X-ray was used to calculate their electronic band structure and the orbital plots. The density functional theory (DFT) calculations[14] were performed on **1**−**2** by using CASTEP code.[15] The total energy was calculated within the framework of the PW91 generalized gradient approximation.[16] The interactions between the ionic cores and the electrons were described by the norm-conserving pseudopotentials.[17] We chose an energy cutoff of the plane-wave of 550 eV and a 4 × 2 × 2 Monkhorst-Pack *k*-point grid for **1**−**2**. To calculate the orbital plots using DMOL2, a generalized gradient approximation (GGA) in the manner suggested by PW91 was applied, and developed by using double numerical plus d-functions basis set.

RESULTS AND DISCUSSION

Synthesis and Mechanism Study. It is well-known that pH value plays an important role in the crystal growth under hydro(solvo)thermal conditions. Inspired by this idea, we proposed to obtain different products by using aqueous ammonia to adjust the pH value of the reaction system involving CuI and L1 in EtOH at 180 °C. As expected, different products can be obtained along with the aqueous ammonia changed from 0.3 to 0.8 mL. A pure phase of **1** was formed with aqueous ammonia used below 0.4 mL; a mixture of **1** and **2** was obtained with aqueous ammonia between 0.5 and 0.6 mL; **2** was isolated as the sole product with aqueous ammonia above 0.7 mL. It is well-known that high-dimensional frameworks are more favored under high pressures. This reaction follows the above-mentioned law, and the dimensions of these two complexes increase from two to three due to the addition of autogenous pressures.

The elemental analyses of **2** clearly show that the 1,3,4-oxadiazole ligand L1 has transformed to triazole and/or triazolate. The X-ray diffraction analysis suggests that the ligand of **2** must has one negative charge to meet the charge balance, and no stretching band of N−H observed in the IR spectrum (Supporting Information Figure S1), indicate that the ligand of **2** is 1,3,4-triazolate. The ^{13}C NMR spectrum (Supporting Information Figure S2) of **2** measured in solid-state due to its poor solubility is consistent with the theoretical values of ^{13}C NMR spectrum given by ChemDraw Ultra 10.0, which further confirm that the ligand of **2** is L2. Due to the symmetry, only four peaks can be observed in the solid-state ^{13}C NMR spectrum of **2**. The peak at 163.7 ppm of ^{13}C NMR spectrum is assigned to the carbon of the 1,2,4-triazolate ring. The chemical shifts of *o*-, *m*-, and *p*-carbon atoms of pyridine are 149.5, 124.6, and 138.9 ppm, respectively. Chen et al. have developed the facile and effective one-pot solvothermal syntheses of 3,5-disubstituted 1,2,4-triazoles through cyclocondensations of organonitriles with ammonia[18] and hydrazine hydrate,[19] respectively. The interesting possible mechanisms have also been deduced from the trapped intermediates by control of the solvothermal conditions and/or the addition of counterions. As an extension of hydro(solvo)thermal metal/ligand reaction of 3,5-disubstituted-1,2,4-triazoles,[20] the in situ copper-mediated ring-to-ring conversion reaction of L1 into L2 is first reported in this work. On the basis of the previously reported literature, a possible mechanism of it is proposed in Scheme 2.[20b,21]

The N atoms at 3 and 4-position of 1,3,4-oxadiazole are first coordinated to Cu ions to form a intermediate (M1), followed by a nucleophilic addition with NH_3 molecules to yield dicopper

diazabutadiene-1,4-diamine tautomer (M2), and then M2 rapidly loses one NH_3 molecule to form 4-H-3,5-bis(4-pyridyl)-1,2,4-triazole copper complex (M3).[21] Finally, the deprotonation of the 4-position N atom of triazole ring meets the charge-balance requirement and leads to the formation of complex **2**.

Structure Description. In the 2-D structure of **1** (Figure 1a), each asymmetric unit consists of three crystallographically independent Cu(I) centers, three iodine ions, and one neutral L1 ligand. The I1 atom adopts a μ_4 mode to bridge four Cu(I) atoms, while I2 and I3 are coordinated to three Cu(I) centers in a μ_3 fashion. The ligand L1 in **1** acts as an angular dipyridyl-like bridge via two terminal pyridyl nitrogen atoms (N1 and N4) to link Cu2 and Cu3 ions, meanwhile, both of which are also bonded to three I atoms to form a slightly distorted $\{CuNI_3\}$ tetrahedral coordination geometry, and whose basal plane is defined by the three I donor (Figure 1b). Cu1 center also adopts distorted tetrahedral coordinated geometry comprised of one μ_3-I2 ion and three crystallographically equivalent μ_4-I1 ions. The distance of Cu(3)−Cu(3A) ~2.7 Å is substantially shorter than the sum of the van der Waals radii (2.8 Å) of Cu(I) centers,[22] indicating Cu(I)···Cu(I) interactions. Both Cu−I (2.6−2.7 Å) and Cu−N (2.0 Å) are in the expected range.[3,23] The torsional angles between the pyridyl rings and the central oxadiazole unit are 9.5(2)° and 7.4(2)°, respectively. The combination of Cu3 and μ_3-I3 generates a 1-D corrugated double-stranded stair-likeinorganic $[CuI]_n$ chain (Figure 1a), and the assembly of Cu1, Cu2, μ_4-I1 and μ_3-I2 forms a 1-D quadruple-stranded zigzag chain containing bowl-shaped Cu_4I_5 moieties (Figure 1c). Interestingly, these two kinds of inorganic chains are linked by angular L1 ligand to generate a 2-D layered framework, in which inorganic chains are parallel to each other and arranged alternately along the *b* axis (Figure 1a). It should be noted that although there are many reports on double-stranded inorganic $[CuX]_n$,[24] to our best knowledge, four-stranded chains of $[CuX]_n$ (X = Cl^-, Br^-, I^-) are very scarce,[25] and **1** represents the first example of concurrence of these two kinds of inorganic $[CuI]_n$ in one structure, according to the Cambridge Crystal Structure Database.

Scheme 2. Possible Mechanism for the Ligand Transformation (M_1−M_3 are Proposed Intermediate)

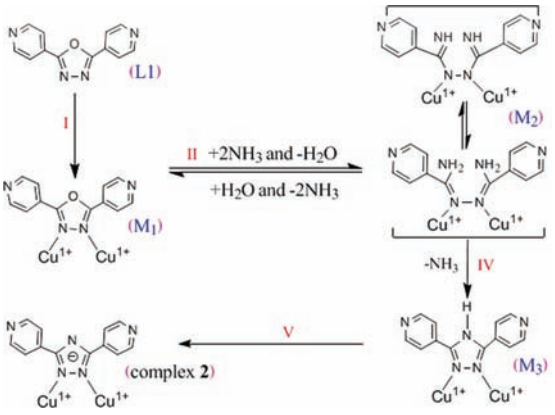

For **2**, the asymmetric unit contains one L2, three crystallographically independent copper(I) centers and two iodine anions. Each iodine atom bridges three copper atoms in a μ_3-bridging mode (Figure 2a). Obviously, **2** has one iodine anion less than **1** in the asymmetric unit, and in order to meet the charge- balance requirement, the neutral ligand L1 is replaced by the one negative charge L2. The L2 ligand acts as a quadridentate bridging linker, coordinating two Cu(I) centers via two terminal pyridyl nitrogens, and further bridge another two Cu(I) atoms via a $\mu_{1,\ 2}$-*N*,*N*′ triazolate. The torsional angles between the pyridyl rings and the central triazolate unit are 21.6 (3)° and 12.6 (3)°, respectively, larger than those of **1**. Both Cu1 and Cu2 adopt trigonal coordinated geometry with copper atoms displaced from the planes by ~0.1 Å. Cu1 center is linked by two μ_3-I2 anions and one N1 atom of triazolate, while Cu2 center is bridged by one μ_3-I2 anions, one terminal nitrogen atom (N5) of pyridyl and one N2 atom of other triazolate, and Cu3 is tetrahedrally coordinated by one terminal pyridyl nitrogen (N4) and three μ_3-I1 anion. Similar to **1**, Cu3 and I1 are arranged to form a corrugated double-stranded stair-shaped inorganic $[CuI]_n$ chains with two different Cu···Cu diagonal distances [Cu(3)−Cu(3A) ≈ 2.7 Å, Cu(3)-Cu(3B) ≈ 2.9 Å] (Figure 2b);

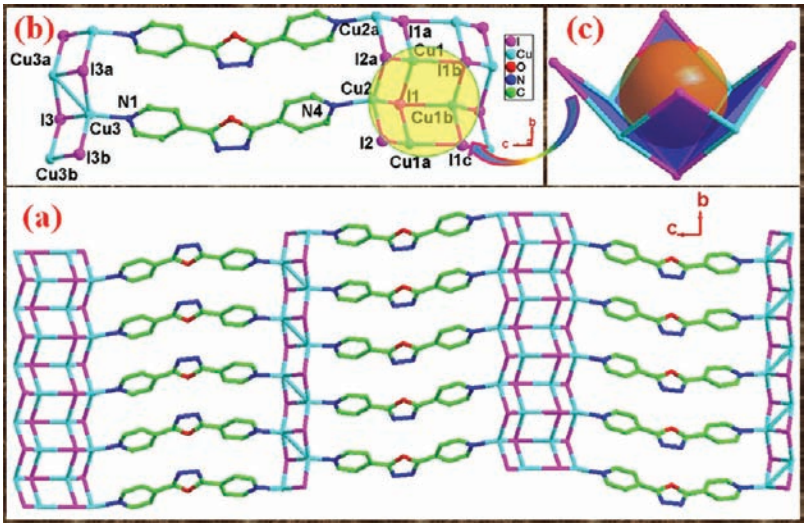

Figure 1. For **1**, (a) perspective view of the 2-D layer with the 1-D corrugated double- and four-stranded stair-like inorganic $[CuI]_n$ chains (hydrogen atoms are omitted for clarity; a, b, c symmetrically generated). (b) Perspective view of coordination environments of Cu atoms and L1. (c) The bowl-like $[Cu_4I_5]$ moiety in four-stranded stair-like inorganic $[CuI]_n$ chains.

dx.doi.org/10.1021/ic2011666 |*Inorg. Chem.* 2011, 50, 11403–11411

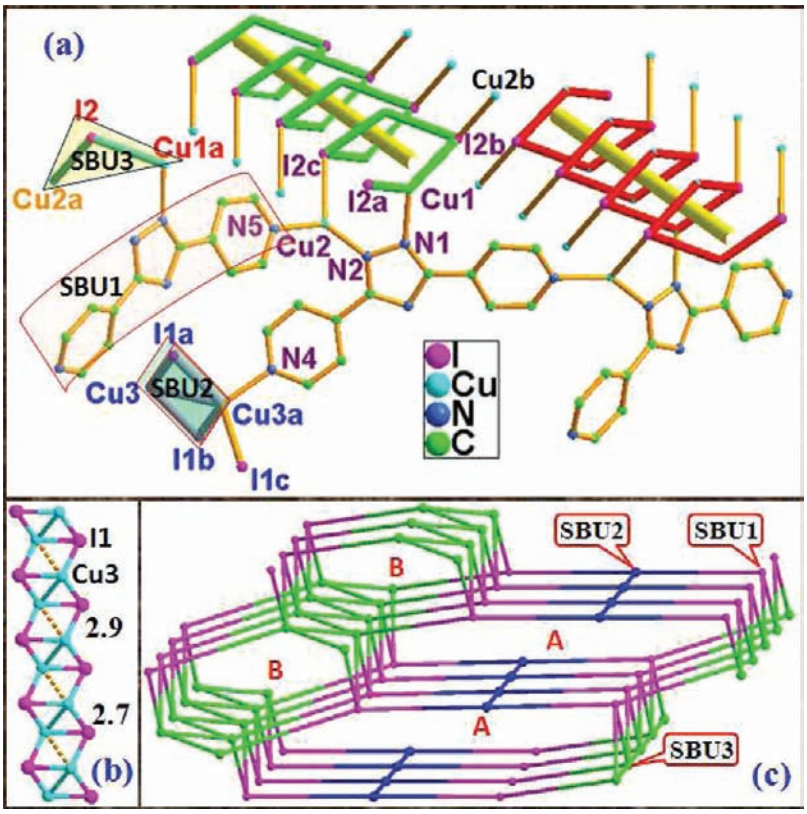

Figure 2. For **2**, (a) perspective view of coordination environment of Cu centers and L2 (hydrogen atoms are omitted for clarity). (b) The 1-D corrugated double-stranded stair-like inorganic $[CuI]_n$ chains. (c) Noninterpenetrating 3-nodal 4,4,5-connected net with two kinds of metallacycle A and B.

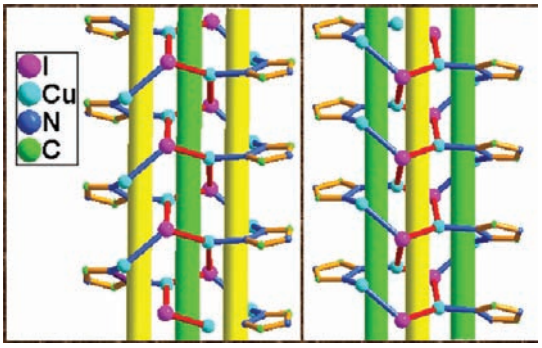

Figure 3. Right-handed three-stranded helical chains (left) and the left-handed three-stranded helical chains (right) in **2**.

however, one striking difference in **2** is that the arrangement of Cu1 and μ_3-I2 leads to an unique single-stranded helical chain running along the crystallographic 2_1 axis, with a short pitch of ~4.1 Å. (Figures 2a and 3). Interestingly, this $[Cu1I2]_n$ helix chain acts as a helical template to link to Cu2 centers through the rest binding sites of μ_3-I2 atoms, and both Cu1 and Cu2 centers are bonded to N atoms at 1- and 2-positions of the triazolate ring to form another two parallel helical chains of the same chirality but opposite to the former $[Cu1I2]_n$ chain, which can be understood as the helix-to-helix induction. Therefore, the chirality of the three-stranded parallel helical chain is opposite to the inorganic $[Cu1I2]_n$ helix chain. The adjacent three-stranded helical chains with opposite chirality are linked by the same

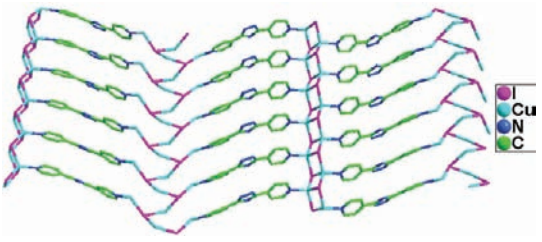

Figure 4. 2-D framework of **2** generated from the 1-D corrugated double-stranded stair-like $[CuI]_n$ inorganic chains and three-stranded helical chains bridged by L2.

ligand L2; consequently, the whole crystal is mesomeric and exhibits no chirality. The linkage between double-stranded inorganic $[CuI]_n$ chains and three-stranded helical chains via the bridge of L2 generates a 2-D corrugated layer (Figure 4). The unsaturated coordination sites of Cu(I) in the three-stranded helical chains are further completed by the triazolate N atoms at 1- and 2-positions, resulting in a complicated 3-D network with two kinds of diamond-like metallacycle A and B along *b* axis (Figures 2c and 5). From the topological point of view, the ligand, the $[Cu3I1]_2$ dimer and the $[Cu1I2Cu2]$ moieties can be regarded as three secondary building units SBU1, SBU2, and SBU3, respectively (Figure 2a). Consequently, the resulted framework is a 3-nodal 4,4,5-connected net topology with Point (Schlafli) symbol: $(4\cdot5^2\cdot6^2\cdot7)(5^4\cdot8^2)(4^3\cdot5\cdot6^6)$ (Figure 2c),[26] in which SBU1 $(4\cdot5^2\cdot6^2\cdot7)$ is connected to one SBU2 $(5^4\cdot8^2)$ and three SBU3 $(4^3\cdot5\cdot6^6)$, and SBU2 is linked to two SBU1 and

dx.doi.org/10.1021/ic2011666 |*Inorg. Chem.* 2011, 50, 11403–11411

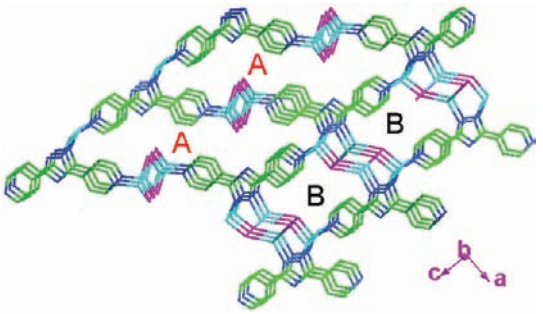

Figure 5. 3-D framework perspective with two kinds of diamond-like metallacycle A and B, viewed along *b*-axis.

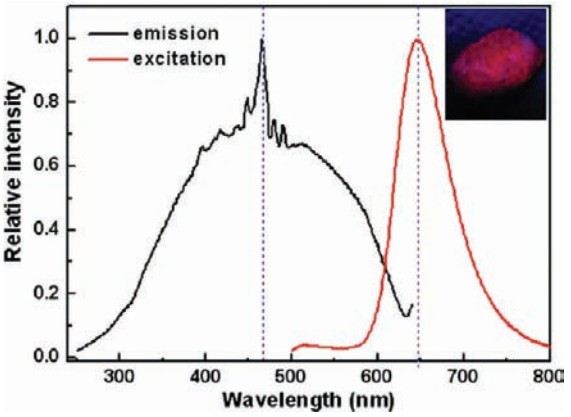

Figure 6. Solid-state electronic emission spectra of complex **1** at room temperature (inset: luminescence photo of complex **1** under ultraviolet light illumination at room temperature).

two itself forming a 1-D corrugated double-stranded stair-like inorganic $[CuI]_n$ chain, while SBU3 is connected to three SBU1 and two itself generating 1-D three-stranded helix chain. It should be pointed out that such topology is unprecedented.

Luminescence and UV−vis-NIR Absorbance Spectra. In the solid state, **1** shows bright red luminescence when excited at 365 nm with a 4 W hand-held UV lamp (Figure 6), and it displays a strong red emission band peaked at ∼648 nm upon photo excitation at ∼465 nm (Figure 6). To the best of our knowledge, this is the first example of red luminescence complex based on 1,3,4-oxadiazole and CuI. The excitation band is very broad (from 300 to 600 nm) with the semipeak to be ∼120 nm, while the emission band is narrow (<100 nm), indicating that the fluorescent color is relatively pure. Besides, their corresponding CIE chromaticity coordinates is (0.66, 0.31), which locates in the pure red color region (Supporting Information Figure S3). It should be mentioned that the luminescent materials with broad band excitation and sharp emission band is very important in flat panel display devices and field emission displays. The lifetime data of the emission can be well fitted by triexponential decay (correlation constants >0.98), giving long multicomponent fluorescent lifetimes parameters (τ_1 = 0.05 μs, 46.74%, τ_2 = 0.13 μs, 42.59%, and τ_3 = 0.01 μs, 10.48%). This implies that there may be two major charge transfer transition in this region. According to previous literature, L1 displays a weak blue fluorescent emission band peaked at ∼470 nm upon photo

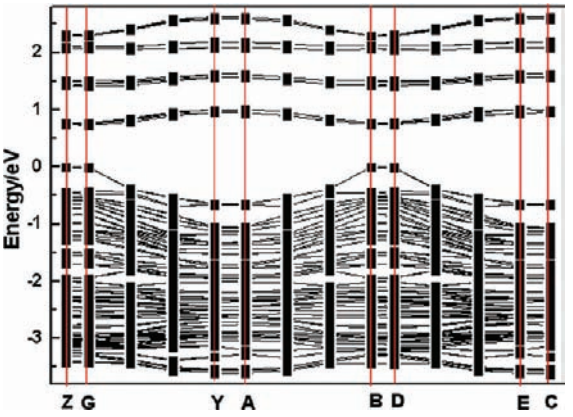

Figure 7. Band structure of **1**. (The Fermi level is set at 0 eV, and the bands below −3.8 eV have been cut for clarity).

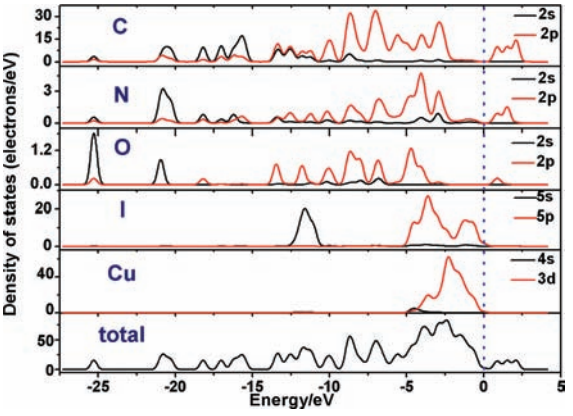

Figure 8. Total and partial density of states for **1**. (The Fermi level is set at 0 eV.)

excitation at ∼300 nm.[27] Compared with L1, the large red shift and enhanced luminous intensity suggest that the luminescence property of the ligand is remarkably affected by the insertion of metal centers giving electronic interaction between the transition metal and the organic ligand framework and contributing to the delocalized π-electron system. The distance of Cu3a−Cu3 (∼2.7 Å) approaches the sum of the van der Waals radii (2.8 Å) of Cu^I centers,[22] as a result, it is difficult to determine whether the metal-centered transitions ^{3}[MC] of the type $3d^{10} \rightarrow 3d^9 4s$ and $3d^{10} \rightarrow 3d^9 4p$ on the copper(I) center[28] or metal−metal bond to ligand charge transfer ^{3}[MMLCT] excited state occurs in **1**. A better insight into the nature of the luminescence property can be achieved by the DFT calculations,[14] which was performed by using CASTEP code.[15] The calculated band structure of **1** along high symmetry points of the first Brillouin zone is plotted in Figure 7, where the labeled *k*-points are present as Z, G, Y, A, B, D, E, and C. It is easy to find that the top of valence bands (VBs) and the bottom of conduction bands (CBs) have small dispersions. The lowest energy (0.78 eV) of CBs and the highest energy (0.00 eV) of VBs are both localized at Z, G, B and D. Accordingly, the present compound shows a semiconducting character with a direct band gap of 0.78 eV (Figure 7), which is smaller than the experimental value 1.86 eV (Supporting Information Figure S4). The deviation of the band gap between the results of semiconductor simulation calculations and experiment is caused by

calculations its own reasons. It is well-known that the GGA are not accurately for treating excited states of semiconductors, which results in the energy level positions of CBs are low and the level positions of the VBs are same with the experimental ones. Therefore, it is not surprising for the calculated band gap is smaller than the experimental value of semiconductors.[29] Investigators have discussed about this study for a long time, however, as an effective approximation method to calculate, the relative value is still accurate, and does not affect the electronic band structure analysis.[30] Based on the total and partial densities of states (DOS) (Figure 8), the band structure of **1** can be assigned. The VBs between energy −5.0 eV and the Fermi level (0.0 eV) are mostly formed by Cu3−3d and I3−5p states, while the CBs between 1.0 and 5.0 eV are almost a contribution from the C-2p, N-2p and O-2p states of L2. In additional, the orbital calculations results indicate that HOMO is mostly composed of the orbitals of Cu3(I) and I3 anions, while LUMO mainly consists of the π^* orbitals of oxadiazole and pyridyl rings (Figure 9). Therefore, these results predict that the emissive excited state of **1** is primarily attributed to the (M + X)LCT state, that is, the charge transitions from Cu3−3d and I3−5p states to C-2p, N-2p and O-2p states.

Electronic Band Structure of 2. The calculated band structure of **2** also shows that the top of valence bands (VBs) and the bottom of conduction bands (CBs) have a small dispersion (Figure 10). The lowest energy (0.92 eV) of CBs and the highest energy (0.00 eV) of VBs are both localized at Z, G, B and D. **2** exhibts a semiconducting character with a direct band gap of 0.92 eV, which is still underestimated but more comparable with the experimental value 1.27 eV than **1** (Supporting Information Figure S4). The bands of **2** can be assigned according to the total and partial densities of states (DOS) (Figure 11). The VBs between energy −5.0 eV and the Fermi level (0.0 eV) are mostly formed by Cu3−3d and I3−5p mixing with a small amount of I3−5s states, while the CBs between 1.0 and 5.0 eV are almost a contribution from the C-2p, N-2p states. In addition, the orbital calculations results indicate that HOMO is mostly composed of Cu3(I) and I1 anions, while LUMO mainly consists of π^* orbitals of triazolate and pyridyl rings (Figure 12) that are connected to the 1-D helix inorganic chain. Therefore it can be considered that the optical absorption of **2** is mainly ascribed to the charge transitions from Cu3−3d and I3−5p mixing with a small amount of I3−5s states to C-2p, N-2p states. It is well-known that for a photovoltaic device such as solar cells with minimal losses, the ideal optical bandgap for maximizing the solar-to-electrical power conversion efficiency is ∼1.1 eV.[31] Therefore, the brown crystal sample **2** with the absorption bands covering the whole UV−vis-NIR spectral region and a band gap of 1.27 eV may be a good potential material for low-voltage solar cells due to the efficient absorption of the majority of the sunlight.[31]

IR Spectra, Thermogravimetric Analysis (TGA), and X-ray Powder Diffraction (XRPD). As shown in Supporting Information Figures S5−7, complexes **1** and **2** were characterized via XRPD and TGA. All the XRPD patterns measured for the as-synthesized samples were in good agreement with the XRPD patterns simulated from the respective single-crystal X-ray data. The thermal stabilities of **1** and **2** were investigated on polycrystalline samples under nitrogen atmosphere from 30 to

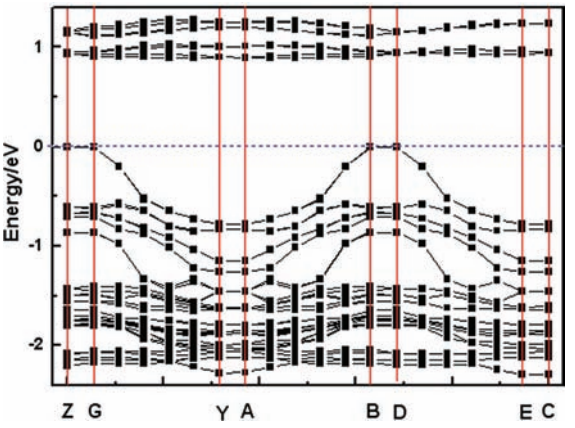

Figure 10. Band structure of **2**. (The Fermi level is set at 0 eV, and the bands below −2.5 eV have been cut for clarity.)

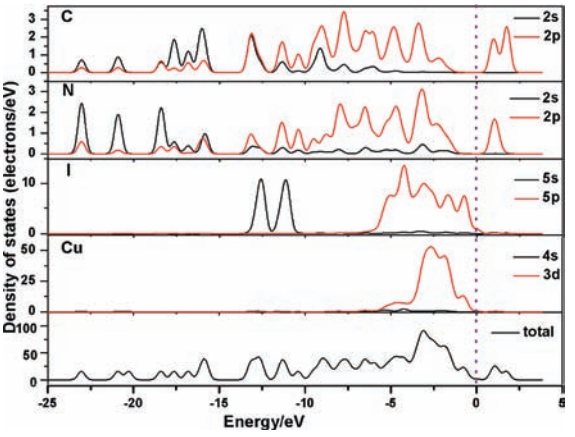

Figure 11. Total and partial density of states for **2**. (The Fermi level is set at 0 eV.)

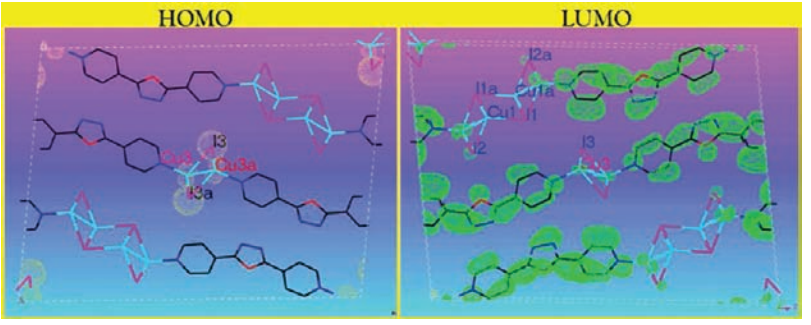

Figure 9. Electron-density distribution of the lowest unoccupied and highest occupied frontier orbitals for **1**.

dx.doi.org/10.1021/ic2011666 |*Inorg. Chem.* 2011, 50, 11403–11411

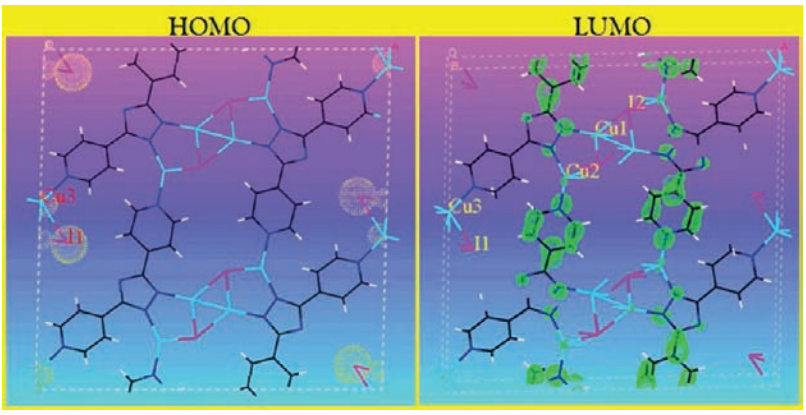

Figure 12. Electron-density distribution of the lowest unoccupied and highest occupied frontier orbitals for **2**.

1200 °C. Complexes **1** and **2** show a similar two-step procedure of weight lost, and start to decompose at 345 and 465 °C, (Supporting Information Figure S7), respectively, indicating that the present complexes are thermally stable for further application.

CONCLUSIONS

In this work, the formation of two novel complexes **1** and **2** in the in situ metal/ligand solvothermal reaction of CuI and L1 can be controlled merely via changing the amount of aqueous ammonia. **1** exhibits 2-D layer containing the parallel and alternately ordered assembled 1-D double- and quadruple-stranded stair-like inorganic $[CuI]_n$ chains, while **2** shows 3-D complicated MOFs consisting of a novel three-stranded helical chains and the same double-stranded $[CuI]_n$ chains as **1**. **2** adopts a novel 3-nodal 4,4,5-connected net topology of an unprecedented Point (Schlafli) symbol: $(4\cdot5^2\cdot6^2\cdot7)(5^4\cdot8^2)(4^3\cdot5\cdot6^6)$. Although both **1** and **2** are built by CuI and the similar ligands, their different structure arrangements of $[CuI]_n$ and ligands result in the different optical properties. **1** displays a strong pure red fluorescent emission band peaked at ~648 nm, while **2** is nonluminescent and the absorption band covers the whole range of UV−vis-NIR spectrum with a band gap of 1.27 eV. **1** is a good potential candidate for hybrid inorganic−organic luminescence materials, and **2** maybe a potential material for a low-voltage solar cells because of the efficient absorption of the majority of the sunlight. In conclusion, the work reported here reveals an intriguing network topology and opens up a promising route for constructing new optical materials that are unattainable through conventional methods.

ASSOCIATED CONTENT

Supporting Information. X-ray crystallographic files in CIF format, solid-state ^{13}C MAS NMR spectra, IR spectra, TG curves, experimental and simulated X-ray powder diffraction patterns for complexes **1**−**2**. This information is available free of charge via the Internet at http://pubs.acs.org.

AUTHOR INFORMATION

Corresponding Author

*Fax: +86-591-83714946; Tel.: +86-591-83705794. E-mail: czlu@fjirsm.ac.cn.

ACKNOWLEDGMENT

This work was supported by the 973 key program of the MOST (2007CB815304, 2010CB933501), the National Natural Science Foundation of China (20873150, 20821061, 20973173, 50772113, and 91022008), the Chinese Academy of Sciences (KJCX2-EW-H01 and KJCX2-YW-M319) and the Natural Science Foundation of Fujian Province(2007HZ0001-1, 2009-HZ0004-1, 2009HZ0006-1, 2006L2005). We are also grateful to Professors Jie Zhang and Jian Zhang for helpful discussions.

REFERENCES

(1) (a) Hoskins, B. F.; Robson, R. *J. Am. Chem. Soc.* **1990**, *112*, 1546. (b) Yaghi, O. M.; Li, H. L.; Davis, C.; Richardson, D.; Groy, T. L. *Acc. Chem. Res.* **1998**, *31*, 474. (c) Batten, S. R.; Robson, R. *Angew. Chem., Int. Ed.* **1998**, *37*, 1460. (d) Zhang, X. M.; Tong, M. L.; Chen, X. M. *Angew. Chem., Int. Ed.* **2002**, *41*, 1029. (e) Yaghi, O. M.; O'Keeffe, M.; Ockwig, N. W.; Chae, H. K.; Eddaoudi, M.; Kim, J. *Nature* **2003**, *423*, 705.

(2) (a) Zhang, Q. C.; Bu, X. H.; Lin, Z.; Biasini, M.; Beyermann, W. P.; Feng, P. Y. *Inorg. Chem.* **2007**, *46*, 7262. (b) Kitagawa, S.; Kitaura, R.; Noro, S. *Angew. Chem., Int. Ed.* **2004**, *43*, 2334. (c) Meng, X. R.; Song, Y. L.; Hou, H. W.; Fan, Y. T.; Li, G.; Zhu, Y. *Inorg. Chem.* **2003**, *42*, 1306. (d) Kondo, M.; Miyazawa, M.; Irie, Y.; Shinagawa, R.; Horiba, T.; Nakamura, A.; Naito, T.; Maeda, K.; Utsuno, S.; Uchida, F. *Chem. Commun.* **2002**, 2156. (e) Lee, S. J.; Hu, A. G.; Lin, W. B. *J. Am. Chem. Soc.* **2002**, *124*, 12948. (f) Zhang, J.; Chen, S. M.; Wu, T.; Feng, P. Y.; Bu, X. H. *J. Am. Chem. Soc.* **2008**, *130*, 12882. (g) Seo, J. S.; Whang, D.; Lee, H.; Jun, S. I.; Oh, J.; Jeon, Y. J.; Kim, K. *Nature* **2000**, *404*, 982. (h) Prins, L. J.; Huskens, J.; de Jong, F.; Timmerman, P.; Reinhoudt, D. N. *Nature* **1999**, *398*, 498. (i) Chin, J.; Lee, S. S.; Lee, K. J.; Park, S.; Kim, D. H. *Nature* **1999**, *401*, 254. (j) Bu, X. H.; Liu, H.; Du, M.; Zhang, L.; Guo, Y. M.; Shionoya, M.; Ribas, J. *Inorg. Chem.* **2002**, *41*, 1855. (k) Wang, X. L.; Chao, Q.; Wang, E. B.; Lin, X.; Su, Z. M.; Hu, C. W. *Angew. Chem., Int. Ed.* **2004**, *43*, 5036. (l) Cui, Y.; Ngo, H. L.; White, P. S.; Lin, W. B. *Chem. Commun.* **2002**, 1666. (m) Chen, X. M.; Liu, G. F. *Chem.—Eur. J.* **2002**, *8*, 4811. (n) Xiong, R. G.; You, X. Z.; Abrahams, B. F.; Xue, Z. L.; Che, C. M. *Angew. Chem., Int. Ed.* **2001**, *40*, 4422. (o) Wang, H. Y.; Cheng, J. Y.; Ma, J. P.; Dong, Y. B.; Huang, R. Q. *Inorg. Chem.* **2010**, *49*, 2416. (p) Liu, Q. K.; Ma, J. P.; Dong, Y. B. *J. Am. Chem. Soc.* **2010**, *132*, 7005. (q) Leroux, Y. R.; Lacroix, J. C.; Chane-Ching, K. I.; Fave, C.; Felidj, N.; Levi, G.; Aubard, J.; Krenn, J. R.; Hohenau, A. *J. Am. Chem. Soc.* **2005**, *127*, 16022. (r) Seminario, J. M.; De La Cruz, C.; Derosa, P. A.; Yan, L. M. *J. Phys. Chem. B* **2004**, *108*, 17879. (s) Lan, A. J.; Li, K. H.; Wu, H. H.; Olson, D. H.; Emge, T. J.; Ki, W.; Hong, M. C.; Li, J. *Angew. Chem., Int. Ed.* **2009**, *48*, 2334. (t) Li, K. H.; Olson, D. H.; Seidel, J.; Emge, T. J.; Gong, H. W.; Zeng, H. P.; Li, J. *J. Am. Chem. Soc.* **2009**, *131*, 10368. (u) Li, K. H.; Lee, J.; Olson, D. H.; Emge, T. J.; Bi, W. H.; Eibling, M. J.; Li, J. *Chem. Commun.* **2008**, 6123.

(3) Knotter, D. M.; Blasse, G.; Vanvliet, J. P. M.; Vankoten, G. *Inorg. Chem.* **1992**, *31*, 2196.
(4) (a) Wong, W. Y.; Liu, L.; Poon, S. Y.; Choi, K. H.; Cheah, K. W.; Shi, J. X. *Macromolecules* **2004**, *37*, 4496. (b) Lindgren, M.; Minaev, B.; Glimsdal, E.; Vestberg, R.; Westlund, R.; Malmstrom, E. *J. Lumin.* **2007**, *124*, 302. (c) Long, N. J.; Williams, C. K. *Angew. Chem., Int. Ed.* **2003**, *42*, 2586.
(5) (a) Nozaki, K. *J. Am. Chem. Soc.* **2006**, *53*, 101. (b) Tsushima, S.; Gotz, C.; Fahmy, K. *Chem.—Eur. J.* **2010**, *16*, 8029. (c) Lazarides, T.; McCormick, T. M.; Wilson, K. C.; Lee, S.; McCamant, D. W.; Eisenberg, R. *J. Am. Chem. Soc.* **2011**, *133*, 350.
(6) (a) Zhang, Q. S.; Ding, J. Q.; Cheng, Y. X.; Wang, L. X.; Xie, Z. Y.; Jing, X. B.; Wang, F. S. *Adv. Funct. Mater.* **2007**, *17*, 2983. (b) Moudam, O.; Kaeser, A.; Delavaux-Nicot, B.; Duhayon, C.; Holler, M.; Accorsi, G.; Armaroli, N.; Seguy, I.; Navarro, J.; Destruel, P.; Nierengarten, J. F. *Chem. Commun.* **2007**, 3077. (c) Zhang, Q. S.; Zhou, Q. G.; Cheng, Y. X.; Wang, L. X.; Ma, D. G.; Jing, X. B.; Wang, F. S. *Adv. Funct. Mater.* **2006**, *16*, 1203. (d) Armaroli, N.; Accorsi, G.; Holler, M.; Moudam, O.; Nierengarten, J. F.; Zhou, Z.; Wegh, R. T.; Welter, R. *Adv. Mater.* **2006**, *18*, 1313. (e) Zhang, Q. S.; Zhou, Q. G.; Cheng, Y. X.; Wang, L. X.; Ma, D. G.; Jing, X. B.; Wang, F. S. *Adv. Mater.* **2004**, *16*, 432.
(7) (a) Kyle, K. R.; Ryu, C. K.; Dibenedetto, J. A.; Ford, P. C. *J. Am. Chem. Soc.* **1991**, *113*, 2954. (b) Kim, T. H.; Shin, Y. W.; Jung, J. H.; Kim, J. S.; Kim, J. *Angew. Chem., Int. Ed.* **2008**, *47*, 685. (c) Tran, D.; Bourassa, J. L.; Ford, P. C. *Inorg. Chem.* **1997**, *36*, 439. (d) Vitale, M.; Ford, P. C. *Coord. Chem. Rev.* **2001**, *219*, 3. (e) De Angelis, F.; Fantacci, S.; Sgamellotti, A.; Cariati, E.; Ugo, R.; Ford, P. C. *Inorg. Chem.* **2006**, *45*, 10576.
(8) (a) Zhang, X. M. *Coord. Chem. Rev.* **2005**, *249*, 1201. (b) Zhang, J. P.; Chen, X. M. *Chem. Commun.* **2006**, 1689. (c) Evans, O. R.; Lin, W. B. *Acc. Chem. Res.* **2002**, *35*, 511. (d) Lu, J. Y. *Coord. Chem. Rev.* **2003**, *246*, 327. (e) Xiong, R. G.; Xue, X.; Zhao, H.; You, X. Z.; Abrahams, B. F.; Xue, Z. L. *Angew. Chem., Int. Ed.* **2002**, *41*, 3800. (f) Zhao, H.; Qu, Z. R.; Ye, H. Y.; Xiong, R. G. *Chem. Soc. Rev.* **2008**, *37*, 84. (g) Xiong, R. G.; Zhang, J.; Chen, Z. F.; You, X. Z.; Che, C. M.; Fun, H. K. *J. Chem. Soc., Dalton Trans.* **2001**, 780. (h) Ma, L. F.; Wang, L. Y.; Du, M. *CrystEngComm* **2009**, *11*, 2593. (i) Zhang, S. Z.; Zhang, Z. H.; Li, C. P.; Du, M. *Inorg. Chem. Commun.* **2009**, *12*, 1038.
(9) (a) Zhang, J. P.; Zheng, S. L.; Huang, X. C.; Chen, X. M. *Angew. Chem., Int. Ed.* **2004**, *43*, 206. (b) Zhang, X. M.; Tong, M. L.; Gong, M. L.; Lee, H. K.; Luo, L.; Li, K. F.; Tong, Y. X.; Chen, X. M. *Chem.—Eur. J.* **2002**, *8*, 3187. (c) Akiya, N.; Savage, P. E. *Chem. Rev.* **2002**, *102*, 2725.
(10) Kang, Y.; Yao, Y. G.; Qin, Y. Y.; Zhang, J.; Chen, Y. B.; Li, Z. J.; Wen, Y. H.; Cheng, J. K.; Hu, R. F. *Chem. Commun.* **2004**, 1046.
(11) Bentiss, F.; Lagrenee, M. *J. Heterocycl. Chem.* **1999**, *36*, 1029.
(12) (a) Wendlandt, W. W.; Hecht, H. G., *Reflectance Spectroscopy*; Interscience Publishers: New York, 1966; (b) Kortüm, G. *Reflectance Spectroscopy*; Springer-Verlag: New York, 1969.
(13) *SHELXTLTM, version 5, Reference Manual*; Science Energy & Automation Inc.: Madison, WI, 1994.
(14) (a) Lee, C. T.; Yang, W. T.; Parr, R. G. *Phys. Rev. B* **1988**, *37*, 785. (b) Wiberg, K. B.; Stratmann, R. E.; Frisch, M. J. *Chem. Phys. Lett.* **1998**, *297*, 60. (c) Wang, C. C.; Yang, C. H.; Tseng, S. M.; Lin, S. Y.; Wu, T. Y.; Fuh, M. R.; Lee, G. H.; Wong, K. T.; Chen, R. T.; Cheng, Y. M.; Chou, P. T. *Inorg. Chem.* **2004**, *43*, 4781. (d) Bauernschmitt, R.; Ahlrichs, R.; Hennrich, F. H.; Kappes, M. M. *J. Am. Chem. Soc.* **1998**, *120*, 5052.
(15) Segall, M. D.; Lindan, P. J. D.; Probert, M. J.; Pickard, C. J.; Hasnip, P. J.; Clark, S. J.; Payne, M. C. *J. Phys.; Condens. Matter* **2002**, *14*, 2717.
(16) Perdew, J. P.; Chevary, J. A.; Vosko, S. H.; Jackson, K. A.; Pederson, M. R.; Singh, D. J.; Fiolhais, C. *Phys. Rev. B* **1992**, *46*, 6671.
(17) Lin, J. S.; Qteish, A.; Payne, M. C.; Heine, V. *Phys. Rev. B* **1993**, *47*, 4174.
(18) Zhang, J. P.; Lin, Y. Y.; Huang, X. C.; Chen, X. M. *J. Am. Chem. Soc.* **2005**, *127*, 5495.
(19) Cheng, L.; Zhang, W. X.; Ye, B. H.; Lin, J. B.; Chen, X. M. *Inorg. Chem.* **2007**, *46*, 1135.
(20) (a) Lu, C. Z.; Fang, Z. L.; Yu, R. M.; Wu, X. Y.; Huang, J. S. *Cryst. Growth. Des.* **2011**, *11*, 2546–2552. (b) Fang, Z. L.; Yu, R. M.; Zhang, J.; Lu, C. Z. *CrystEngComm* **2011**, *13*, 4032–4038.
(21) (a) Kauffman., T; Albrecht, J.; Berger, D.; Legler, J. *Angew. Chem., Int. Ed.* **1967**, *6*, 633.
(22) Bondi, A. *J. Phys. Chem.* **1964**, *68*, 441.
(23) (a) Garland, M. T.; Lemarouille, J. Y.; Spodine, E. *Acta Crystallogr., Sect. C* **1985**, *41*, 855. (b) Buchanan, R. M.; Wilsonblumenberg , C.; Trapp, C.; Larsen, S. K.; Greene, D. L.; Pierpont, C. G. *Inorg. Chem.* **1986**, *25*, 3070.
(24) (a) Wu, T.; Li, M.; Li, D.; Huang, X. C. *Cryst. Growth Des.* **2008**, *8*, 568. (b) Song, R. F.; Xie, Y. B.; Li, J. R.; Bu, X. H. *CrystEngComm* **2005**, *7*, 249.
(25) Wu, T.; Li, D.; Ng, S. W. *CrystEngComm* **2005**, *7*, 514.
(26) (a) Domasevitch, K. V.; Solntsev, P. V.; Gural'skiy, I. A.; Krautscheid, H.; Rusanov, E. B.; Chernega, A. N.; Howard, J. A. K. *J. Chem. Soc., Dalton Trans.* **2007**, 3893. (b) Min, T. Y.; Zheng, B.; Bai, J. F.; Sun, R.; Li, Y. Z.; Zhang, Z. X. *CrystEngComm* **2010**, *12*, 70.
(27) Mahmoudi, G.; Morsali, A. *CrystEngComm* **2007**, *9*, 1062.
(28) (a) Palmer, C. E. A.; Mcmillin, D. R.; Kirmaier, C.; Holten, D. *Inorg. Chem.* **1987**, *26*, 3167. (b) Horvath, A.; Zsilak, Z.; Papp, S. *J. Photochem. Photobiol. A: Chem.* **1989**, *50*, 129. (c) Chermette, H.; Pedrini, C. *J. Chem. Phys.* **1981**, *75*, 1869. (d) Pedrini, C. *Phys. Status Solidi B* **1978**, *87*, 273.
(29) (a) Terki, R.; Bertrand, G.; Aourag, H. *Microelectric Eng.* **2005**, *81*, 514. (b) Aguilera, I.; Palacios, P.; Wahnon, P. *Thin Solid Films* **2008**, *516*, 7055. (c) Shay, J. L.; Wernick, J. H., *Ternary Chalcopyrite Semiconductors: Growth Electronic Properties and Applications*, Pergamon Press, Oxford, 1974.
(30) (a) Stampfl, C.; Van de Walle, C. G. *Phys. Rev. B* **1999**, *59*, 5521. (b) Norman, M. R.; Perdew, J. P. *Phys. Rev. B* **1983**, *28*, 2135.
(31) (a) Shockley, W.; Queisser, H. J. *J. Appl. Phys.* **1961**, *32*, 510. (b) Snaith, H. J. *Adv. Funct. Mater.* **2010**, *20*, 13.